INL/CON-11-20932
PREPRINT

Design of an Annular Linear Induction Pump for Nuclear Space Applications

Nuclear and Emerging Technologies for Space 2011

Carlos O. Maidana
James E. Werner
Daniel M. Wachs

February 2011

The INL is a
U.S. Department of Energy
National Laboratory
operated by
Battelle Energy Alliance

Proceedings of Nuclear and Emerging Technologies for Space 2011
Albuquerque, NM, February 7-10, 2011
Paper 3236

Design of an Annular Linear Induction Pump for Nuclear Space Applications

Carlos O. Maidana[1], James E. Werner[1] and Daniel M. Wachs[1]

[1] *Idaho National Laboratory, Space Nuclear Systems and Technology Division, Idaho Falls, ID 83415-3855, USA*
e-mail of contacting author: maidana@physics.isu.edu

Abstract. The United States Department of Energy's (DOE) Office of Nuclear Energy, Science, and Technology is supporting the National Aeronautics and Space Administration (NASA) in evaluating space mission power, propulsion systems and technologies to support the implementation of the Vision for Space Exploration (VSE). NASA will need increased power for propulsion and for surface power applications to support both robotic and human space exploration missions. As part of the Fission Surface Power Technology Project for the development of nuclear reactor technologies for multi-mission spacecrafts, an Annular Linear Induction Pump, a type of Electromagnetic Pump for liquid metals, able to operate in space has to be designed. Results of such design work are described as well as the fundamental ideas behind the development of an optimized design methodology. This project, which is a collaboration between Idaho National Laboratory (INL), Pacific Northwest National Laboratory (PNNL) and Marshall Space Flight Center (MSFC), involves the use of theoretical, computational and experimental tools for multi-physics analysis as well as advanced engineering design methods and techniques.

Keywords: Annular Linear Induction Pump, Electromagnetic Pump, Space Nuclear Systems, MHD.

INTRODUCTION AND FUNDAMENTALS

The design process and technology evaluation of annular linear induction pumps (ALIP) was divided in three stages. The first stage is a basic study of the main electrical, mechanical and thermal parameters which constitute the basis of this paper. The second stage is the fabrication and test of a full scale prototype to characterize the pump performance. The third stage is the comparison of the actual construction parameters and test results against the developed models and designed parameters for the future design and construction of an optimized ALIP for nuclear space applications.

Working Fundamentals

The ALIP under design make use of a 3-phase alternate current input voltage to power a group of solenoids that generates a traveling magnetic field along the pump duct, Fig. 1. This traveling magnetic field induces a current on the surface of the liquid metal in the duct and as a result, an electromagnetic (EM) force is generated. This EM force will be the one pumping the molten metal through the duct.

One can model the current, I, of the primary windings by an equivalent current sheet at the outer wall of the pump[1]:

$$J_s(z,t) = J_a e^{i(\omega t - kz)} \tag{1}$$

where k = π/τ, τ is the pole pitch, ω is the angular frequency, $J_a = 3\sqrt{2}kNI/p\tau$, p the number of pole pairs and N is the number of turns per slot. This is a sinusoidal wave with wavelength L and speed, or synchronous velocity, $v_b=\omega L/2\pi$; the pole pitch being $\tau=L/2$ and the length $L=2p\tau$.

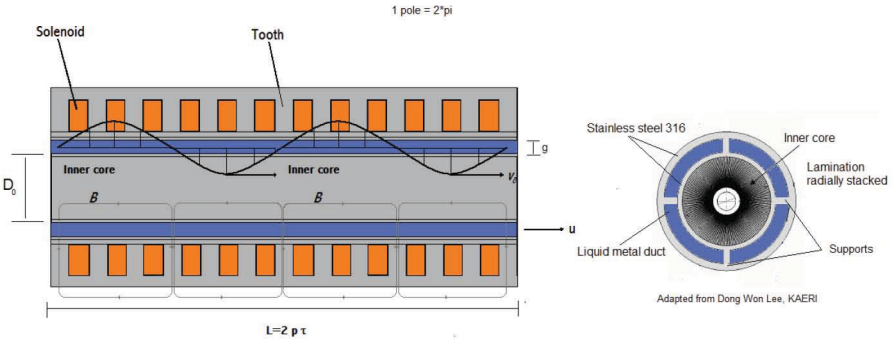

Figure 1: Cross sections of an annular linear induction pump.

The equations describing the pumping process in the duct are [2]:

$$\boldsymbol{J_i} = \sigma(\boldsymbol{E}+\boldsymbol{u}\times\boldsymbol{B}) \tag{2}$$

$$\rho\left[\frac{\partial \mathbf{u}}{\partial t} + (u\cdot\nabla)\mathbf{u}\right] + \nabla p - \rho\nu\nabla^2\mathbf{u} - \mathbf{f} = \mathbf{J}\times\mathbf{B} \tag{3}$$

where the current density is $\mathbf{J}=\mathbf{J}_s+\mathbf{J}_i$, σ and ν are the conductivity and kinematic viscosity (ratio of the viscous force to the inertial force) of the fluid, and **u** is the fluid velocity. Because the linear momentum of the fluid element could change not only by the pressure force, $-\nabla p$, viscous friction, $\rho\nu\nabla^2\vec{\boldsymbol{u}}$, and Lorentz force, $\vec{\boldsymbol{J}}\times\vec{\boldsymbol{B}}$, but also by volumetric forces of non electromagnetic origin, eq. (3) has the addition of the term $\boldsymbol{f}$; while the conservation of mass for liquid metals is given by $\nabla\cdot\vec{\boldsymbol{u}}=\mathbf{0}$, which expresses the incompressibility of the fluid. An induction equation, valid in the domain occupied by the fluid and generated by the mechanical stretching of the field lines due to the velocity field, can be written as,

$$\frac{\partial}{\partial t}\boldsymbol{B} + (\boldsymbol{u}\cdot\nabla)\boldsymbol{B} = \frac{1}{\mu\sigma}\nabla^2\boldsymbol{B} + (\boldsymbol{B}\cdot\nabla)\boldsymbol{u}\,, \tag{4}$$

describing the time evolution of the B field, $\partial\boldsymbol{B}/\partial t$, due advection $(\boldsymbol{u}\cdot\nabla)\boldsymbol{B}$, diffusion $\nabla^2\boldsymbol{B}$ and field intensity sources $(B\cdot\nabla)\boldsymbol{u}$. The term $(\mu\sigma)^{-1}$ is known as magnetic diffusivity. One of the solutions of the induction equation gives rise to the possibility of self-excitation of the $\boldsymbol{B}$ field even with no external field sources due to small perturbations once the production of magnetic intensities by mechanical stretching overcomes their damping by diffusion. The induction equation, eq. (4), can be written dimensionless by the introduction of scale variables, one of such variables is the magnetic Reynolds number, $R_m = \mu\sigma L u_0$, where u_0 is the mean velocity and L the characteristic length. A relatively small R_m generates only small perturbations on the applied field; if R_m is relatively large then a small current creates a large induced B field. For small Reynolds numbers (R_m<<1), the magnetic field will be dominated by diffusion and perturbative methods can be used. Expressing the magnetic Reynolds number as $R_m = (g/\delta_m K_c)\cdot(\sigma\mu\omega/k^2)\cdot s$ where δ_m is the wall thickness (non-magnetic gap), K_c is the Carter's coefficient and s the slip factor[3], it was found experimentally that instabilities arises when the following three conditions hold true: $R_{ms}>1$, the ratio of the mean radius to the pole pitch ($D/2\tau$) and the modified interaction parameter N_{int} are large enough. The modified interaction parameter is expressed as $N_{int}=2gB_{ar}^2\,\sigma/\rho\lambda v_b$ where B_{ar} is the radial component of the applied magnetic field and λ the friction coefficient. This instability appears as a low frequency pulsation in the pressure head affecting the flow rate, liquid metal velocity and magnetic field distribution. As a consequence vortices are generated in the inlet region as well as

fluctuations in the winding currents and voltages. Araseki et al.[3] have reported that the dominant frequency of this instability is in the range 0-10 Hz with amplitude that increases with the slip factor.

In a similar way, one can find that the equation for temperature is

$$\rho c_p \left[\frac{\partial}{\partial t}\boldsymbol{T} + (\boldsymbol{u}\cdot\nabla)T\right] = \nabla\cdot(\lambda\nabla\boldsymbol{T}) + \frac{1}{\sigma}\boldsymbol{J}^2 + \Phi + Q \ , \tag{5}$$

which is a convection-diffusion equation with λ: thermal conductivity, Q: other sources of volumetric energy release such as radiation or chemical reactions and thermal diffusivity κ: $\lambda/\rho c_p$, c_p: constant pressure specific heat of the flow; while the kinetic energy evolution is given by,

$$\frac{\partial}{\partial t}\left(\frac{1}{2}\rho u^2\right) = -\nabla\cdot\left[\boldsymbol{u}\left(p+\frac{1}{2}\rho u^2\right) - \boldsymbol{u}\cdot\boldsymbol{S}\right] + \boldsymbol{u}\cdot(\boldsymbol{J}\times\boldsymbol{B}) + \boldsymbol{u}\cdot\boldsymbol{f} - \Phi \ , \tag{6}$$

where **S** is the viscous stress tensor, which is related to the deformation tensor **D**, by the constitutive equation **S** = 2ν**D**. The variable Φ is the vector dissipation term, **S**:**D**. The deformation tensor can be expressed as $\boldsymbol{D} = [D_{ij}] = \frac{1}{2}\left[\frac{\partial u_i}{\partial x_j} + \frac{\partial u_j}{\partial x_i}\right]$. We deduce from the latter that due to the action of the Lorentz forces an increase of the kinetic energy leads to a decrease in the magnetic energy. From the temperature equation, eq. (6), one can identify the temporal increase of enthalpy, $\rho c_p \frac{\partial T}{\partial t}$, which equals to the loss of magnetic energy due to joule dissipation, $\frac{1}{\sigma}J^2$, plus the loss of kinetic energy, Φ, due to viscous dissipation. The ratio of kinetic energy to the accumulated energy can be expressed through the so called *Eckert number*, E_c, which can be expressed numerically as $E_c = \frac{u_0^2}{c_p \Delta T_0}$, where the subscript indicates average or core values. The *Eckert number* could be useful to express dissipation.

Specific working Requirements

The EM pump under design has the following requirements: an operating temperature between 850 and 875 K, an initial pressure of 20 psi (137895 Pa) and a pressure head of 3-6 psi (20684 Pa); A compound of 78% K and 22% Na known as NaK78 will be the working fluid with a flow rate of 4.3 kg/s (5.03 10^{-3} m^3/s). Since the NaK thermal conductivity is so high, the principal mode of energy transfer is conduction, and not convection. The ALIP will be part of a cooling system for a fast spectrum reactor intended for a lunar surface power system and will be required to operate in a vacuum environment.

The working fluids considered were Na, Li and NaK78. The disadvantage of NaK78 compared to the other options is the fact that it requires more pumping power than Na or Li but when we study other characteristics we find a series of advantages that NaK78 has over the other elements, among them:

- NaK78 is liquid at 261K while Li at 454K and Na at 361K;
- Li dissolves Ni at the temperature of interest so it is not suitable to use with steels or super-alloys;
- Neutron capture of ^{6}Li and ^{7}Li produces He gas that would have to be removed from the reactor;
- NaK78 activates less strongly than Na.

DESIGN METHODOLOGY

There are many possibilities to design, model and simulate EM pumps and its components. Some main parameters can be obtained by decoupling the electrodynamics from the thermo-fluid component. The parameters obtained are first order approximations and they constitute the basis for a qualitative understanding of the physical phenomena taking place.

Electric Circuit Model Approach

The idea behind the equivalent circuit approach relies on the assumption that the flow is laminar (pressure and velocity independent of time). Hence the electromagnetic and hydrodynamic phenomena can be separated. Then the theory of linear induction machines and electric circuits can be used[5], Fig. 2a). It is assumed that only one phase needs to be considered (symmetry of a 3-phase balanced system). Using this approach the flow rate, Q, and the developed pressure, ΔP, are connected by the following expression[5]:

$$\Delta P = \frac{3I^2}{Q}\frac{R_2(1-s)}{s\left(\frac{R_2^2}{X_m^2 s^2}+1\right)}, \tag{7}$$

where X_m is the magnetizing reactance of the pump, R_2 the secondary resistance due to the liquid metal and s is the slip factor (1- $u_{liq.\ metal}$/ $u_{\text{traveling wave}}$). An alternative expression[1,4] is:

$$\Delta P = \frac{36\sigma s f \tau^2 (\mu_0 k_w N I)^2}{p g_e^2\{\pi^2+(2\mu_0\sigma s f \tau^2)^2\}}, \tag{8}$$

where g_e is the effective inter-core gap coefficient (K_c*g, K_c: Carter coefficient and g: inter-core gap), τ is the pole pitch, p the number of pole pairs, N the number of turns per slot, k_w the winding coefficient, f the input frequency and μ_0 the vacuum magnetic permeability. The resistance of the liquid metal can be expressed[5] as,

$$R_2 = \frac{6\pi D \rho_r' (k_w N)^2}{\tau p}, \tag{9}$$

as well as the magnetizing reactance of the pump,

$$X_m = \frac{6\mu_0 \omega \tau \pi D_0 (k_w N)^2}{\pi^2 p g_e}, \tag{10}$$

where ρ_r' is the surface resistivity of the fluid (resistivity/fluid thickness), D_0: diameter of the inner core, D: mean diameter of the fluid and g_e: effective inter-core gap (g_e= Carter's coefficient*inter core gap). Another important parameter is the pump efficiency. In a very first approximation[6], it can be expressed as

$$\eta = \frac{\Delta P \cdot Q}{3VIP_f}, \tag{11}$$

where V is the phase voltage and P_f is the power factor. But a more useful expression for pump design[7] is,

$$\varepsilon = \frac{6k_w^2(1-s)}{\frac{\rho_c N_{coils,pole,ph} k_p^2 N_{ph}^2 \sigma g_e}{k_f k_d \tau}\left\{1+\left(\frac{\pi}{2\mu_0 f s \sigma \tau^2}\right)^2\right\}+\frac{6k_w^2}{s}}, \tag{12}$$

where k_f: slot filling factor (usually 0.5 to 0.6), k_d: slot depth/width, N_{ph}: number of input phases and k_p: slot pitch/slot width. In a similar way, another expression for the developed pressure can be derived,

$$\Delta P = \frac{18I^2}{Q}\frac{\pi D \rho_r' \mu_0 f (k_w N)^2 s(1-s)}{3\pi^2 D \rho_r' g_e (k_w N)^2 + \tau^3 \mu_0 p f s^2}, \tag{13}$$

where $\tau = L/(2p)$. These equations were confirmed experimentally for Na with accuracy of 7% to 17%. Main contributors to the uncertainties are the end effects generated by the distortion of the magnetic fields at both ends of the pump. Using the Kim-Baker-Tessier method, the width of the stator slot is given by

$$D_{stator\ slot} = 0.625\frac{\tau}{N_{phases} N_{coils,pole,phase}}, \tag{14}$$

where N_{phases} is the number of phases and $N_{coils,\ pole,\ phase}$ is the number of coils per pole per phase. In a similar way, the width of the stator tooth is given by

$$D_{stator\ tooth} = 0.375\frac{\tau}{N_{phases}N_{coils,pole,phase}}\ , \tag{15}$$

Being the slot depth five times the stator slot width ($D_{slot\ depth} = 5D_{stator\ slot}$).The clearance between the coil and the end of the stator tooth was estimated to be ~2.54 mm for a voltage of 120 V. The winding distribution factor, k_w, can be expressed as

$$k_w = \frac{\sin(180°/2N_{phases})}{N_{coils,pole,phase}sin(180°/2N_{phases}N_{coils,pole,phase})}\ . \tag{16}$$

The maximum value of the developed force increases with the diameter of the inner core and the efficiency decreases for larger inner core diameters. The lower the input frequency and the longer the core length, the larger the maximum value of the efficiency. The number of turns should be moderate so as not to require values of the input voltage which are too large due to the increased impedance that results from a large number of turns.

Heat Transfer Considerations, Materials and Related Issues

The material selected for the ALIP ducts and outer shell is 316 stainless steel. Grade 316 is the standard molybdenum-bearing grade, which gives it a better overall corrosion resistant property than grade 304. The austenitic structure gives it good toughness properties in a wide range of temperature. The inner core and stator material could be laminated silicon steel which has anisotropic heat conductivity, Fig. 1b. The heat conductivity in the lamination plane is 5 to 30 times higher than the component in the stacking direction. The laminated material reduces the losses produced by the induced eddy currents. For acceptable losses, flux density swing ΔB must be restricted to much less than the magnetic flux density at the material saturation limit[8], B_{sat}.

$$\Delta B = \frac{1}{N \cdot A_e}\int E\ dt\ , \tag{17}$$

where N is the number of turns, A_e the core cross section and E dt is the applied voltage per second. ΔB is the total peak flux swing whereas ΔB/2 should be applied in the core loss curves.

One option for the coil conductors is alumina-dispersed-strengthened Cu strip conductors, which has a small volume expansion coefficient, with HML coating plus double glass insulation, Si impregnated and one layer Si bonded mica tape all around the coil. The selected material for this application is glidcop AL-15, which is a low alumina content grade of dispersion strengthened Cu consisting of a pure Cu matrix containing finely dispersed sub-microscopic particles of Al_2O_3 which act as a barrier to dislocation movement. The dispersed Al_2O_3 is thermally stable so that it acts to retard recrystallization of the Cu. Consequently, significant softening does not occur as the result of high temperature exposure. Along with superior strength retention, thermal and electrical conductivities are higher than conventional Cu alloys.

Another material to consider is ceramic aluminum nitrate which is not only a good electrical insulator but a good thermal conductor as well. Aluminum nitride is used to fill the space between stator, coils and outer shell. Ceralloy 1370-DP is a good option of ceramic aluminum nitrate.

Three phase power system

The ALIP under design make use of a 3-phase alternate current input voltage to power the group of solenoids that generates the traveling magnetic field along the pump duct. The system is assumed to be

balanced so only one-phase needs to be considered. The coils can be interconnected in either "Y" or "Δ" configuration. The Δ configuration is the most common but the values of the equivalent one-phase circuit correspond to the equivalent "Y" configuration. A diagram of a "Δ" configuration is shown in Fig. 2b).

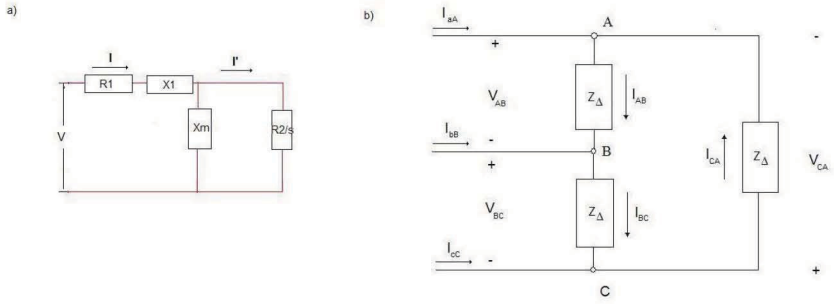

Figure 2: a) Equivalent circuit for the ALIP, b) Equivalent circuit diagram for a "Δ" configuration interconnection.

In a balanced system, the currents $I_{aA}=I_{bB}=I_{cC}$; so if current measurements indicate otherwise the system is not balanced and that might be an indication of damage or fabrication flaws in the solenoids; I_{aA}, I_{bB}, I_{cC} are known as the line currents, I_{line} ; I_{AB}, I_{BC}, I_{CA} are known as the phase currents, I_{phase} . The relationship between currents is $I_{line} = \sqrt{3} I_{phase}$ with a change in phase of 30^0. In a load connected in "Δ", $V_{line}=V_{phase}$. The power associated to each phase is $P_A=P_B=P_C=P_{phase}=V_{phase}I_{phase}\cos(\theta)$, where θ is the angle between the phase voltage and the phase current. The total power to a balanced "Δ" load would be

$$P_{total} = 3P_{phase} = 3V_{phase}I_{phase}cos(\theta) = \sqrt{3}V_{line}I_{line}\cos(\theta) \ , \tag{18}$$

For the analysis of the one-phase "Y" equivalent circuit the equivalent impedance is $Z_Y=(1/3)Z_\Delta$. If the voltage taken is $V_{A\text{-gnd}}$ then $V_{AB} = \sqrt{3}V_{A-gnd}$ (30^0 phase shift). A 3-phase power system under balanced operation has the property that the instantaneous power is constant in value. As a consequence, the ALIP exhibits less vibration and noise than a mono-phase device. The power source of the ALIP should be able to generate a sine wave signal to drive the solenoids; if the power source cannot generate a high fidelity sine wave then a sine wave filter should be used. Since nonlinear components generate harmonic currents, any distortion of an originally pure sine wave constitutes harmonic frequencies. When the sine-wave distortion is symmetrical above and below the average centerline of the waveform, the only harmonics present will be odd-numbered. The 3rd harmonic, and integer multiples of it, are known as triplen and they are in phase with each other, despite the fact that their respective fundamental waveforms are 120 degrees out of phase with each other. Triplen harmonic currents in a "Δ" connected set of components circulate within the loop formed by the "Δ".

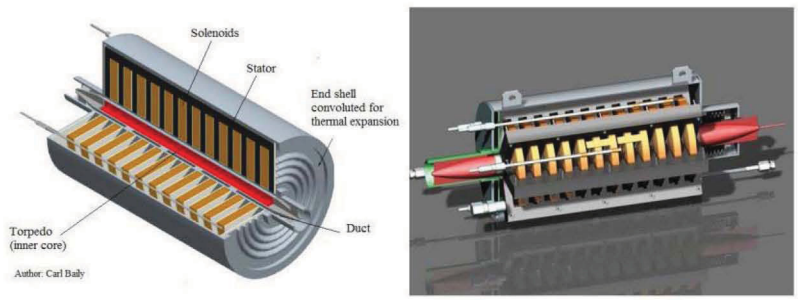

Figure 3: 3D model of the EM pump. Notice how the inner core, or torpedo, extends beyond the solenoid-stator section.

The three-phase winding arrangement for the solenoids usually follows the sequence AA ZZ BB XX CC YY where A, B, C denote the balanced three-phase winding and X, Y, Z the opposite phase; for a direct balanced system, if A: 0 deg, B:120 deg and C:240 deg then X:180 deg, Y:300 deg and Z:60 deg. Arranging the sequence by rising phase, one obtain the correct winding sequence for the solenoids: AA ZZ BB XX CC YY. Sometimes a phase shift to this arrangement could minimize certain instabilities present in the pump but a lower efficiency of the ALIP is the cost to pay for such procedure.

FURTHER CONSIDERATIONS

Construction approaches & operational issues

Using the methodologies just explained, a first set of parameters for the ALIP design was obtained and two models were generated, Fig. 3. In the Kim-Baker-Tessier (KBT) approach there is a thermal insulation between the duct and the solenoids, some cooling gas space and a k_d: slot depth/width factor of 1.6. In the Adkins-INL approach there is no thermal insulation between the duct and the solenoids but a high thermal conductor/high dielectric in contact with the duct and a k_d factor of 1.85 was chosen.

Studies have established a limit to the temporal variation in temperature. The pump should not be heated at a rate larger than 1-16 C per minute. The thickness of the duct walls affect the efficiency of the pump due to the magnetic resistivity that presents; but it must not be too thin as too risk its structural integrity. The width of the fluid channel should be limited to below the skin depth of the fluid for stable operation.

$$skin\ depth = \delta = \frac{1}{\sqrt{\pi f u \sigma}} \tag{19}$$

End effects

The fringe fields generated by coils contain various nonlinearities due to the longitudinal dependence of the magnetic field. Due to the solenoids fringe fields, its finite core length and the induced currents, the ALIP has an *end effect* at both ends of the pump. A reduction on the developed force arises which is roughly equal to the product of the magnetic field and its perpendicular induced current. Theoretical calculations indicate a reduction of the end effects by controlling the input frequency; increasing the efficiency at the lower frequencies compared with results obtained at frequencies over 60 Hz. The inlet *end effect* force affects most of the pump while the outlet *end effect* domain is limited to the exit region. Considering the direct relationship between fluid velocity and *end effect*, low frequency operation is preferred as far as the developing force and the efficiency are not decreased too much. When the end effects are neglected, it is easy to show that the pump efficiency is given as the ratio of the flow velocity u to the synchronous velocity ω/κ of the fields (i.e. $n=\kappa u/\omega=1-s$). But when the end effects are included its efficiency has to be computed using numerical integration and its maximum lies in the range $0.2<s<0.4$.

Instabilities and flow

As explained before, instabilities arise when the three conditions hold true: $R_{ms}>1$, $D/2\tau$ and N_{int} = *"large enough"*. An instability appears as a low frequency (LF) pulsation in the pressure head affecting the flow rate, liquid metal velocity and magnetic field distribution. As a consequence vortices are generated in the inlet region as well as fluctuations in the winding currents and voltages. The dominant frequency of this instability is in the range 0-10 Hz with amplitude that increases with the slip factor. This LF pressure pulsation is produced by vortices in the liquid metal generated by the no uniformity of the azimuthal component of the applied magnetic field when $R_{ms}>1$. The magnetic Reynolds number, R_{ms}, often

becomes greater than unity in the pump region where the slip is larger than 0.2 giving place to another instability known as double supply frequency (DSF) pressure pulsation. The vibration caused by the DSF pressure pulsation occurs in the pump outlet and propagates to the pipe when $R_{ms}<1$ and $s<0.2$[3].

CONCLUSIONS

A first study for the design of an annular linear induction pump for space applications was done using different theoretical models, experimental data and computational tools. Very few information is available on this topic and there is a lack of a full theoretical understanding of the processes involved that constitute a problem for an accurate design procedure. Another problem relies in the non-existence of solvers for the engineering magnetohydrodynamic analysis the FSP technology project needs to perform. Some of these problems are being addressed by the authors of this paper and the results of our first study were used for a qualitative understanding of the parameters involved in the design process and as a basis for the generation of more accurate models. The different physical phenomena involved cannot always be decoupled and therefore a more precise multi-physics analysis constitutes a priority. A test model was built at the U.S. Department of Energy's Idaho National Laboratory together with a test loop at one of NASA's test facilities, a series of experiments were designed, software is being tested and different mathematical and computational methods are being studied with the goal of developing a set of programs, algorithms and methodologies for ALIPs design and optimization. These tasks contribute to the evaluation process for space fission power and propulsion systems and technologies for space exploration.

ACKNOWLEDGMENTS

Prepared for the National Aeronautics and Space Administration and for the U.S. Department of Energy under DOE Idaho Operations Office contract DE-AC07-OSID14157.

REFERENCES

1. CHO, S. et al., "*The magnetic field and performance calculations for an electromagnetic pump of a liquid metal*," J. Physics D: Appl. Phys. 31 (1998).

2. BORGHI, C. A. *et al.*, "*Study of the Design model of a Liquid Metal Induction Pump*," IEEE Transactions on Magnetics, Vol. 34, N 5, September 1998.

3. ARASEKI, H. *et al.*, "*Magnetohydrodynamic instability in annular linear induction pump. Part I & II. Experiment and numerical analysis*," Nuclear Engineering and Design 227, Elsevier (2004).

4. GERBEAU, J., "*Mathematical Methods for the Magnetohydrodynamics of Liquid Metals*," Oxford University Press, 2006.

5. MULLER, U., Buhler, L., "*Magnetohydrodynamics on Channels and Containers*," Springer, 2001.

6. KIM, H., "*Design and Experimental Characterization of an EM Pump*," Journal of the Korean Physical Society, 35/4, 1999.

7. KIM, H. R. et al., "*Development and Verification of Design Code for Small Annular Linear Induction EM Pump*," The Korean Nuclear Society Spring Meeting, Pohang University, May 1999.

8. TEXAS INSTRUMENTS, "*Technical notes for the design of high frequency transformers*," 1996.

9. BAKER, R. S. and Tessier, M. J., "*Handbook of Electromagnetic Pump Technology*," Elsevier, 1987.

10. MAIDANA, C. O., "*Design Of A Cabinet Safe System For A Portable Particle Accelerator*", VDM Verlag, 2009.